Robotics and Computer-Integrated Manufacturing 28 (2012) 437–448

Contents lists available at SciVerse ScienceDirect

Robotics and Computer-Integrated Manufacturing

journal homepage: www.elsevier.com/locate/rcim

Workspace analysis of 5-PRUR parallel mechanisms (3T2R)

Mohammad Hossein Saadatzi [a], Mehdi Tale Masouleh [b,*], Hamid D. Taghirad [a]

[a] Advanced Robotics & Automated Systems, Faculty of Electrical & Computer Engineering, K.N. Toosi University of Technology, P.O. Box 16315-1355, Tehran, Iran
[b] Department of Mechatronics Engineering, Faculty of New Sciences & Technologies, University of Tehran, P.O. Box 1374-14395, Tehran, Iran

ARTICLE INFO

Article history:
Received 16 July 2011
Received in revised form
4 December 2011
Accepted 22 December 2011
Available online 25 January 2012

Keywords:
5-DOF parallel mechanisms
Constant-orientation workspace
Three translational and two rotational (3T2R) motion pattern
CAD model
Geometric constructive approach
Bohemian dome

ABSTRACT

This paper investigates the constant-orientation workspace of five-degree-of-freedom parallel mechanisms generating the three translations and two independent rotations and comprising five identical limbs of the PRUR type. The general mechanism was proposed recently from the type synthesis performed for 5-DOF parallel mechanisms with identical limb structures. In this study, the emphasis is placed on the determination of the constant-orientation workspace using a geometric interpretation of the so-called vertex space, i.e., the motion generated by a limb for a given orientation. The geometric investigation is carried out using geometric constructive approach, which is implemented in a computer algebra system and in a CAD system. This paper shows that these two approaches are complementary tools to investigate the workspace of parallel mechanisms. The geometric constructive approach proposed in this paper bring insight into the architecture optimization and it can be regarded as a guideline for the workspace analysis of parallel mechanisms whose vertex spaces generate Bohemian dome.

1. Introduction

Due to some remarkable kinematic properties, parallel manipulators have stimulated the interest of researchers and industries and they have been extensively synthesized using intuition and ingenuity. The development of the systematic type synthesis of parallel mechanisms [1] channels researchers to synthesize parallel mechanisms with fewer than six degrees of freedom (DOF), referred to as lower mobility mechanisms. As far as 5-DOF parallel mechanisms with identical limb structures (PMILS) are concerned, researchers have mainly worked on the type synthesis [1–6]. It is worth noticing that most existing 5-DOF parallel mechanisms, omitting the hybrid mechanisms [7], are built using a 5-DOF constraining leg, referred to as passive leg, which constrains some actuated 6-DOF limbs [8–10], which are referred to as a limited-DOF parallel mechanisms with non-identical limb structures. Recently, the type synthesis of 5-DOF parallel mechanisms, have been revised [1–6] and Huang and Li [11] and Liu et al. [12] proposed a first architecture.

Since, in the industrial context, the 3T2R motion can cover a wide range of applications including, among others, 5-axis machine tools and welding, therefore, in this research, the kinematic properties of this class of mechanisms will be investigated [13–16]. The kinematic properties of 5-DOF PMILS performing the 3T2R motion pattern are still not well understood and there are many issues which should inevitably be addressed including the constant-orientation workspace and forward kinematic problem (FKP) [17–23].

There has been a vast literature on various approaches to obtain and optimize their workspace which ranges from discretization algorithms to geometrical approaches [24]. In the majority of cases, the complete workspace of spatial parallel mechanisms is embedded into a six-dimensional space for which no visualization exists or which is extremely difficult to assess geometrically. To circumvent this problem, sections with fixed translation or rotation of the complete workspace are proposed. The focus of this paper is on a commonly used such section: the constant-orientation workspace. The constant-orientation workspace consists of the set of feasible positions of the mobile platform for a prescribed orientation of the platform.

While most of the literature propounded on this topic is based purely on numerical methods [25–30], including the continuation method and interval analysis [24,31,32], we advocate the need for a revival of the geometric approaches to obtain the constant-orientation workspace which, in general, is twofold:

1. Geometric constructive approach.
2. CAD-based modelling approach.

Both approaches presented above are to the majority of intents and purposes the same and in our case they only differ from their way to formulate the problem, reason for which we consider

* Corresponding author.
E-mail addresses: mhsaadatzi@ieee.org (M.H. Saadatzi), mehdi.tale-masouleh.1@ulaval.ca (M. Tale Masouleh), taghirad@kntu.ac.ir (H.D. Taghirad).

0736-5845/$ - see front matter © 2011 Elsevier Ltd. All rights reserved.
doi:10.1016/j.rcim.2011.12.002

them complementary rather than counterpart. There are host of considerations relevant to choosing an approach, such as the availability of the required CAD software (SolidWorks system is used here) or the computer algebra system (like MATLAB software), for the computation of the constant-orientation workspace of complex mechanisms and they are well discussed in [33,34].

In what concerns the geometric constructive approach, in this paper, the problem is investigated upon following the reasoning proposed in [35] for the constant-orientation workspace analysis of 6-DOF parallel mechanisms whose vertex space is a sphere. Two important features of the method are its low computational time [36] and the possibility to readily find the volume of the workspace. Emerging here is the notion of the *vertex space* which is the motion generated by one limb constituting the parallel mechanism for a prescribed orientation of the mobile platform.

This can be achieved by inspiring the mathematical formulation proposed in [35]. However, the approaches proposed in [35] cannot be used directly to obtain the constant-orientation workspace of a large class of parallel mechanisms, especially those obtained recently using the type synthesis [1], for which:

1. The topology of the vertex space is not defined from the outset and does not correspond to a simple pre-defined geometric object, such as a sphere in the case of Gough–Stewart platform and a circle in the case of a 3-RPR parallel mechanism.
2. The horizontal and vertical cross-sectional planes of the vertex space do not result in homogeneous sections to which algebraic equations can be associated, such as circles.

To circumvent these problems, in this paper, the geometric constructive approach is divided into two steps: geometric constructive approach of the vertex space (GCAV), and geometric constructive approach of the constant-orientation workspace (GCACOW).

As a second approach, the CAD-based modelling approach, an in-depth geometric inspection of the vertex space topology is performed. This gives a proper insight into design of the mechanisms under study and the obtained topology, which can be extended to other types of mechanisms revealed in [1], can be made equivalent to a quadric surface called *Bohemian* dome. The main challenge in obtaining the topology of the vertex space is the extension of Bohemian domes to the final vertex space, which should be performed by considering particular cases and the stroke of the actuators. Due to some limits of the CAD systems in generating complex geometric objects, the extension of the Bohemian dome into the vertex space, which can be regarded as an extrusion of the Bohemian dome along an axis, cannot be done in one single step and several successive steps are required to do so.

It can be shown that the vertex space of some of the mechanisms proposed in [1] for 4- and 5-DOF PMILS can be made equivalent to a Bohemian dome, such as the 4-ŔŔŔŔR̀ ≡ 4-RPUR and 4-ŔR̀R̀ŔŔ ≡ ŔR̀UŔ, and the algorithm proposed in this paper can be extended for them. Here and throughout this paper, R, P, U and C stand, respectively, for the revolute, prismatic, universal and cylindrical joint and the underlined joint is activated. In the case of C joint, the prismatic joint is activated. It should be noted that the mechanism under study in this paper, i.e., the 5-PRUR parallel mechanism can be regarded as one of the most difficult one which makes its workspace analysis to be considered as a guideline for other mechanisms having Bohemian dome as vertex space. Also, it is worth mentioning that the proposed methods in this paper can be verified easily by using discretization method for the 5-PRUR and other parallel mechanisms.

The remainder of this paper is organized as follows. First, the architecture and the general kinematic properties of the 5-PRUR parallel mechanism which originated from the type synthesis performed in [1] are outlined. The IKP and two general classes for PRUR arrangement are reviewed. The constant-orientation workspace is interpreted geometrically and the results are implemented in a CAD system. More emphasis is placed on the geometric constructive approach of the workspace carried out by computer algebra systems, GCAV and GCACOW, and the CAD model of the workspace. Finally, based on the latter algorithm, the volume of the constant-orientation workspace is obtained and plotted with respect to the two permitted rotational DOFs.

2. Architecture review and kinematic modelling of the 5-PRUR parallel mechanisms

Figs. 1 and 2 provide, respectively, representations of two possible arrangements for a PRUR limb and a schematic representation for a 5-DOF parallel mechanism, called *Pentapteron* [1,5] which was first

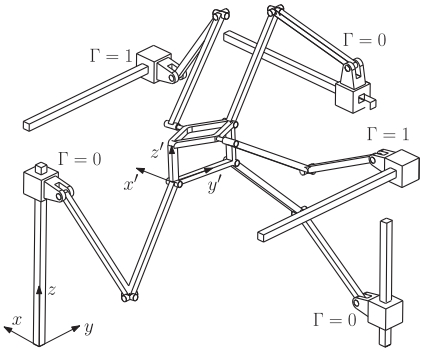

Fig. 2. Schematic representation of Pentapteron, a 5-DOF (3T2R) parallel mechanism.

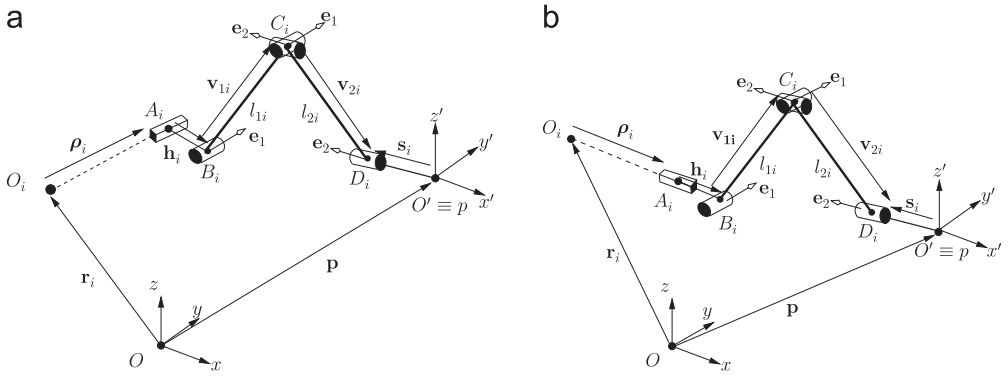

Fig. 1. Schematic representation of (a) CUR ≡Γ=1 and (b) PRUR ≡Γ=0.

revealed in [37] where the corresponding kinematic arrangement of the limbs is fully described.

Such a mechanism can be used to produce all three translational DOFs, plus two independent rotational DOFs (3T2R) of the end-effector, namely (x,y,z,ϕ,θ). In the latter notation, (x,y,z) represent the translational DOFs with respect to the fixed frame O, illustrated in Fig. 2, and (ϕ,θ) stand, respectively, for the orientation DOFs around axes x and y. In addition, the axes of the first R joints in all the legs are arranged to be parallel to the direction of a group of two of the linearly actuated joints. Therefore, two types of kinematic arrangements are possible, as depicted in Fig. 1, for the legs: (a) the parallel type, Fig. 1(a), and (b) the perpendicular type, Fig. 1(b). In fact, $\Gamma=0$ and $\Gamma=1$ differ in some kinematic properties such as constant-orientation workspace and the inverse kinematic problem (IKP) formulation. It is noted that Γ designates the cosine of the angle between the prismatic actuator axis and the first R joint axis.

The rotation from the fixed frame O_{xyz} to the moving frame $O'_{x'y'z'}$ is defined as follows: a first rotation of angle ϕ is performed around the x-axis followed by the second rotation about the y-axis by angle θ. The latter leads to the following rotation matrix:

$$\mathbf{Q}=\begin{bmatrix}\cos\theta & \sin\phi\sin\theta & \cos\phi\sin\theta\\ 0 & \cos\phi & -\sin\phi\\ -\sin\theta & \sin\phi\cos\theta & \cos\phi\cos\theta\end{bmatrix}. \tag{1}$$

In this paper the superscript $'$ for a vector stands for its representation in the mobile frame. In a 5-PRUR parallel mechanism, the axes of all the R joints are always parallel to a plane defined by its normal vector $\mathbf{e}_3=\mathbf{e}_1\times\mathbf{e}_2$ where $\mathbf{e}_1$ and $\mathbf{e}_2$ are unit vectors defining the direction of the R joints. From *screw theory*, it follows that the mechanism has no possibility to perform a rotation about an axis which is orthogonal to a plane spanned by $[\mathbf{e}_1,\mathbf{e}_2]$. From a practical point of view, for the proposed architecture vectors $\mathbf{e}_1$ and $\mathbf{e}_2$ are orthogonal.

3. IKP of the 5-PRUR parallel mechanism

In the ith leg, the motion of the actuated prismatic joint is measured with respect to a reference point A_i, located on the direction associated with the prismatic actuator. Vector $\mathbf{e}_{\rho i}$ is in turn defined as a unit vector in the direction of the prismatic joint and therefore the vector connecting point O_i to point A_i can be written as $\boldsymbol{\rho}_i=\rho_i\mathbf{e}_{\rho i}$. Vector $\mathbf{r}_i$ is defined as the position vector of point O_i, the starting point of the prismatic actuator, in the fixed reference frame. Similarly, vector $\mathbf{s}_i$ is the vector connecting point O' of the platform to a reference point D_i on the axis of the last revolute joint of the ith leg. Point C_i is defined as the intersection of the axes of the second and third revolute joints of the ith leg. Vectors $\mathbf{v}_{1i}$ and $\mathbf{v}_{2i}$ are, respectively, the vector connecting point B_i to point C_i and point C_i to D_i.

Finally, the position of the platform is represented by vector $\mathbf{p}=[x,y,z]^T$ connecting point O to point O' and the orientation of the moving frame with respect to the fixed frame is given by a rotation matrix $\mathbf{Q}$. For a given value of the angles ϕ and θ, matrix $\mathbf{Q}$ is readily computed and vectors $\mathbf{s}_i$ can obtained as

$$\mathbf{s}_i=\mathbf{Q}\mathbf{s}'_i. \tag{2}$$

With reference to Fig. 1, the following equations, arising from the kinematic constraint of the ith limb, can be written as

$$(x_{Ci}-x_{Bi})^2+(z_{Ci}-z_{Bi})^2=l_{1i}^2, \tag{3}$$

$$(x_{Di}-x_{Ci})^2+(y_{Di}-y_{Ci})^2+(z_{Di}-z_{Ci})^2=l_{2i}^2, \tag{4}$$

$$(x_{Di}-x_{Ci})\cos\theta-(z_{Di}-z_{Ci})\sin\theta=0 \tag{5}$$

such that the first two equations represent, respectively, the magnitude of $\mathbf{v}_{1i}$ and $\mathbf{v}_{2i}$ and the last one corresponds to the kinematic constraints between $\mathbf{e}_2$ and $\mathbf{v}_{2i}$, i.e., $\mathbf{e}_2\perp\mathbf{v}_{2i}$. The solution of the IKP is different for each case, i.e., $\Gamma=1$ and $\Gamma=0$, and requires to be investigated separately.

3.1. Solution of the IKP for $\Gamma=1$

In this case, Eqs. (3)–(5) should be solved for $y_{Ci}={}^{y}\rho_i$ for a given pose of the platform. Having in mind that for $\Gamma=1$ one has $y_{Ci}=y_{Bi}={}^{y}\rho_i$, then the coordinate of point C_i is unknown for the IKP. Thus by eliminating passive variables, and skipping mathematical details, it follows that the IKP formulation can be divided into two expressions for two different sets of working modes:

$${}^{y}\rho_i=y_{Di}+\delta_{1i}\sqrt{l_{2i}^2-({}^{1}K'_i)^2}, \tag{6}$$

$${}^{y}\rho_i=y_{Di}+\delta_{1i}\sqrt{l_{2i}^2-({}^{2}K'_i)^2}, \tag{7}$$

where

$${}^{1}K'_i=|\mathbf{v}_i\cdot\mathbf{e}_3|-\sqrt{l_{1i}^2-(\mathbf{a}_i\cdot\mathbf{e}_2)^2},\quad {}^{2}K'_i=|\mathbf{v}_i\cdot\mathbf{e}_3|+\sqrt{l_{1i}^2-(\mathbf{a}_i\cdot\mathbf{e}_2)^2} \tag{8}$$

and

$$\mathbf{a}_i=\mathbf{s}_i+\mathbf{p}-\mathbf{r}_i. \tag{9}$$

In the above, $\delta_{1i}=\{-1,1\}$ stands for the two working modes. From the above expressions it can be deduced that the IKP admits up to four solutions. From a geometric stand point, as depicted in Fig. 3 which results in two solutions, the IKP resolution for a $\Gamma=1$ limb can be made equivalent to the intersection of a cylindrical surface and a circle whose axes are orthogonal.

From the compact and rigorous formulation found for the IKP we gain insight into the boundary curves of the limb which prepares the essentials for the first step toward the constant-orientation workspace analysis of the 5-PRUR parallel mechanisms. Boundary curves of a limb can be identified mathematically by inspecting the conditions for which the IKP looses its capability to produce real solutions. To lay down the essential tools for the workspace analysis, we start to formulate the conditions for which the IKP solutions for a given limb are on the verge of having real solutions and to satisfy the corresponding stroke of the actuator. These conditions are based on the inequality constraints of the IKP, plus the inequalities expressing the stroke of

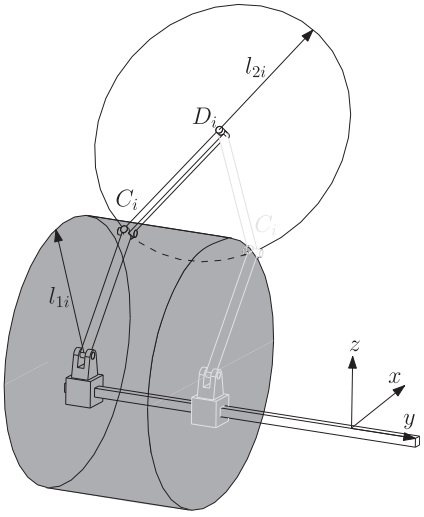

Fig. 3. Configuration which results in two solutions for the IKP of $\Gamma=1$.

the actuator which can be written as

$$K_{1i} \geq 0 \quad K_{1i} = l_{1i}^2 - (\mathbf{a}_i \cdot \mathbf{e}_2)^2, \tag{10}$$

$$K_{2i} = l_{2i}^2 - ({}^1K_i')^2 \geq 0, \tag{11}$$

$$K_{3i} = l_{2i}^2 - ({}^2K_i')^2 \geq 0, \tag{12}$$

$$K_{s_i} = \frac{\Delta\rho_i}{2} - |{}^y\rho_i - y_{Ai}| \geq 0. \tag{13}$$

The first one, K_{1i}, should hold in order to have the primary condition for having a real solution for the IKP and a pose which fails to satisfy this condition will be definitely out of the reachable region of the limb, regardless the stroke of the actuator. The next two, K_{2i} and K_{3i}, are governing the number of the solutions to be either two or four where upon each satisfaction two solutions are generated. The fourth one, K_{s_i}, has the role to determine whether the prismatic actuator is within the range of the motion defined by its stroke, $\Delta\rho_i = \rho_{\max\, i} - \rho_{\min\, i}$.

3.2. Solution of the IKP for $\Gamma = 0$

Let us consider the case for which the prismatic actuator is along the x-axis, in which case its elongation is denoted as ${}^x\rho_i$, based on the defined convention. As it can be observed, Eqs. (3)–(5) contain passive variables, $C_i(x_{Ci},y_{Ci},z_{Ci})$ and $D_i(x_{Di},y_{Di},z_{Di})$, which are, respectively, the coordinates of the passive U and the last R joints. Using the fact that the last R joint is attached to the platform, the coordinate of point D_i can be related to the pose of the platform. Upon eliminating the above passive variables from the system of equations presented in Eqs. (3)–(5) and by skipping mathematical details, the following is obtained for the IKP:

$${}^x\rho_i = x_{Di} + \delta_{0i} \sin\theta\sqrt{K_i} + \upsilon_{0i}\sqrt{l_{1i}^2 - (z_{Di} + \delta_{0i}\cos\theta\sqrt{K_i} - z_{Bi})^2}, \tag{14}$$

where $\delta_{0i} = \{-1, 1\}$ and $\upsilon_{0i} = \{-1, 1\}$ stand for the two different working modes and:

$$K_i = l_{2i}^2 - (y_{Di} - y_{Ci})^2. \tag{15}$$

An analogous approach leads to obtaining the IKP when the prismatic actuator is along z-axis, denoted as ${}^z\rho_i$:

$${}^z\rho_i = z_{Di} + \delta_{0i}\cos\theta\sqrt{K_i} + \upsilon_{0i}\sqrt{l_{1i}^2 - (x_{Di} + \delta_{0i}\sin\theta\sqrt{K_i} - x_{Bi})^2}. \tag{16}$$

From $\delta_{0i} = \{-1, 1\}$ and $\upsilon_{0i} = \{-1, 1\}$, which stand for representing different working modes, it follows that the IKP admits up to four real solutions and $4^5 = 1024$ for the mechanisms as a whole. Fig. 4 shows a configuration for which the IKP admits four solutions.

In order to set down gradually the essentials for the workspace analysis, which is the matter of the next section, the boundary curves for $\Gamma = 0$ are obtained. By the same reasoning as for $\Gamma = 1$, the boundary curves of $\Gamma = 0$ are:

1. For ${}^x\rho_i$:

$$K_{1i} = K_i \geq 0, \tag{17}$$

$$K_{2i} = l_{1i}^2 - (z_{Di} - \cos\theta\sqrt{K_i} - z_{Bi})^2 \geq 0, \tag{18}$$

$$K_{3i} = l_{1i}^2 - (z_{Di} + \cos\theta\sqrt{K_i} - z_{Bi})^2 \geq 0, \tag{19}$$

$$K_{s_i} = \frac{\Delta\rho_i}{2} - |{}^x\rho_i - x_{Ai}| \geq 0. \tag{20}$$

2. For ${}^z\rho_i$:

$$K_{1i} = K_i \geq 0, \tag{21}$$

$$K_{2i} = l_{1i}^2 - (x_{Di} - \sin\theta\sqrt{K_i} - x_{Bi})^2 \geq 0, \tag{22}$$

$$K_{3i} = l_{1i}^2 - (x_{Di} + \sin\theta\sqrt{K_i} - x_{Bi})^2 \geq 0, \tag{23}$$

$$K_{s_i} = \frac{\Delta\rho_i}{2} - |{}^z\rho_i - z_{Ai}| \geq 0. \tag{24}$$

4. From the vertex space to the workspace analysis of 5-PRUR parallel mechanisms

Geometrically, the problem of determining the constant-orientation workspace for a limb of the 5-PRUR parallel mechanism can be regarded as follows: For a fixed elongation of the prismatic actuator, the first revolute joint provides a circular trajectory centred at A_i with l_{1i} as radius. The second link generates a surface by sweeping a second circle, with $\mathbf{e}_2$ as axis and l_{2i} as radius, along the first circle. Since the direction of $\mathbf{e}_2$ is prescribed and must remain constant, the surface obtained is quadratic and is called a *Bohemian dome*.

This quadratic surface can be obtained by moving a circle that remains parallel to a plane along a curve that is perpendicular to the same plane, as shown in Fig. 5. Once this surface is obtained, it should be extended in such a way that it represents the vertex space of the limb for different elongations of the prismatic actuators with respect to its stroke $\Delta\rho_i$. The main challenge in obtaining the topology of the vertex space of a PRUR limb is to find a general, complete and systematic procedure to extend the Bohemian dome to the vertex space. As mentioned above, $\Gamma = 0$ and $\Gamma = 1$ have different IKP formulations and vertex space topologies. Moreover, the vertex space of each case falls into different classes depending on the values of l_{1i}, l_{2i} and $\Delta\rho_i$. In

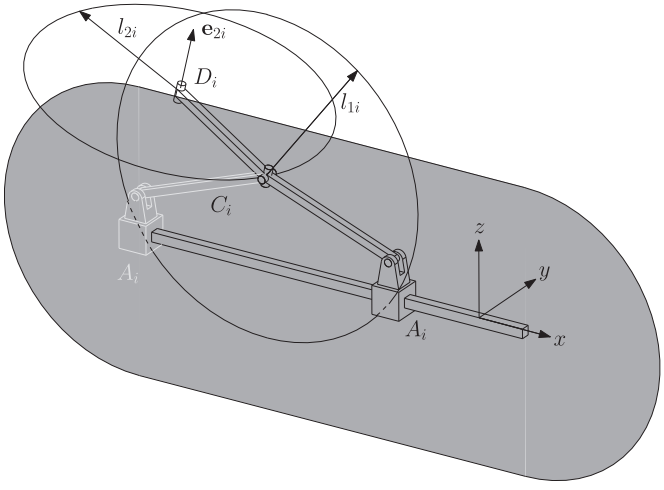

Fig. 4. Configuration which results in four solutions, only two are shown for clarity, for the IKP of $\Gamma = 0$ with prismatic actuator along the x-axis.

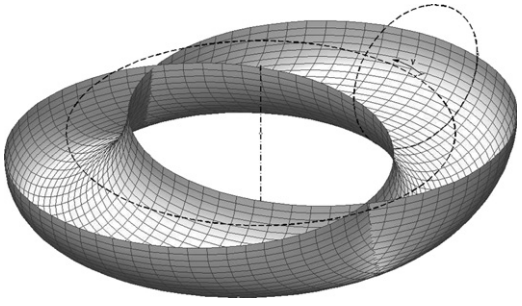

Fig. 5. The lower half of a Bohemian dome. The representation is taken from [38].

what concerns the rotational parameters, (ϕ,θ), only θ influences the vertex space topology, since the axis $\mathbf{e}_2$ which defines the angle θ is located intermediately in the limb, in contrast to ϕ which is remote to the platform. The influence of l_{1i}, l_{2i}, $\Delta\rho_i$ and θ on the vertex space is the main reason that makes difficult the geometric assessment of the vertex space of a PRUR limb. In the following section, first, the topology of the vertex space, for both cases $\Gamma=\{0,1\}$, is elaborated and then the constant-orientation workspace is investigated.

Before presenting the details related to the construction of the CAD model of the vertex space, the complexity of the model is discussed briefly. In fact, θ is the rotation angle around axis $\mathbf{e}_1$, which is in the direction of the y-axis. Thus in the case for which the prismatic actuator is along the y-axis, i.e., $\Gamma=1$, the vertex space for different angles θ can be obtained by applying a rotation around the prismatic actuators axis by θ. It is apparent that the latter rotation preserves the direction of the prismatic actuator. Thus for $\Gamma=1$ once the vertex space for $\theta=0$ is in hand then it can be readily extended to different values of θ. By contrast, the vertex space of $\Gamma=0$ cannot be modelled readily in such a way that covers different θ since rotating the vertex space obtained for $\theta=0$ for $\Gamma=0$ around $\mathbf{e}_1$ does not preserve the direction of the prismatic actuator. In what concerns the second alternative toward obtaining the boundary of the vertex space, a geometrical constructive approach is used, called the geometric constructive approach of the vertex space (GCAV).

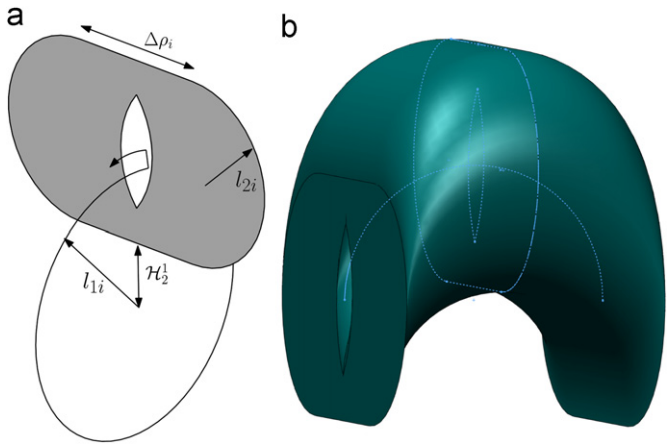

Fig. 6. Vertex space for $\Gamma=1$ having both holes $\mathcal{H}_1^1$ and $\mathcal{H}_2^1$. (a) Schematic model. (b) CAD model.

4.1. Topology of the vertex space for $\Gamma=1$

4.1.1. CAD-based modelling approach

Having determined that for a fixed prismatic actuator and fixed θ both $\Gamma=\{0,1\}$ generate a Bohemian dome, the next step consists in extending this surface in such a way that results in a general model of the vertex space which considers the stroke of the actuator plus θ. For $\Gamma=1$, one should first consider the motion generated by the second moving link for which the $\Delta\rho_i$ is considered. This surface is represented in Fig. 6(a) as a shaded surface. Directly from Fig. 6, it follows that two distinct types of holes can appear in the extension from Bohemian dome to the vertex space of $\Gamma=1$:

1. A throughout hole called $\mathcal{H}_1^1$: when $\Delta\rho_i < l_{2i}$.
2. A side hole called $\mathcal{H}_2^1$: when $l_{2i} < l_{1i}$.

Thus from the above, the topology of the vertex space for $\Gamma=1$ falls into four cases:

1. $\mathcal{G}_{01}$: $\Delta\rho_i \geq l_{2i}$ and $l_{2i} \geq l_{1i}$, none of the holes appear.
2. $\mathcal{G}_{02}$: $\Delta\rho_i \geq l_{2i}$ and $l_{2i} \leq l_{1i}$, only $\mathcal{H}_2^1$ appears.
3. $\mathcal{G}_{03}$: $\Delta\rho_i < l_{2i}$ and $l_{2i} \geq l_{1i}$, only $\mathcal{H}_1^1$ appears.
4. $\mathcal{G}_{04}$: $\Delta\rho_i < l_{2i}$ and $l_{2i} < l_{1i}$, both $\mathcal{H}_1^1$ and $\mathcal{H}_2^1$ appear.

Fig. 7 demonstrates the four different vertex spaces belonging to $\Gamma=1$. From the latter figure it can be observed how $\mathcal{H}_1^1$ and $\mathcal{H}_2^1$ may influence the vertex space. It can be readily deduced that an optimal design for a $\Gamma=1$ corresponds to $\mathcal{G}_{01}$. All the vertex spaces depicted in Fig. 7 correspond to a configuration for which $\theta=0$. As mentioned previously, vertex spaces for different values of θ for $\Gamma=1$ can be obtained by applying a rotation about the axis of the prismatic actuator by θ.

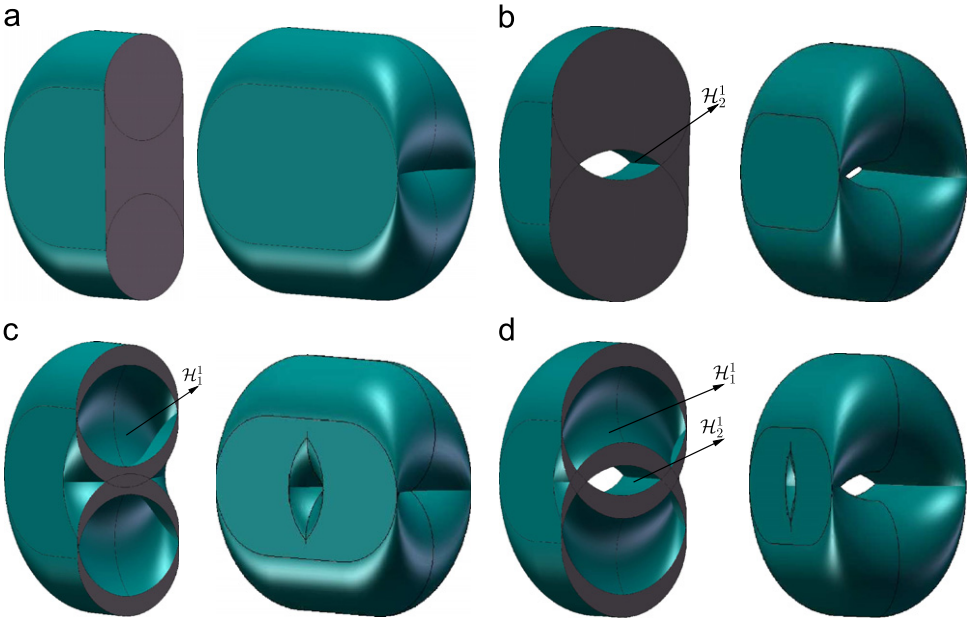

Fig. 7. CAD model of the vertex space for $\mathcal{G}_{0i}$, $i=1,\ldots,4$. (a) $\mathcal{G}_{01}$. (b) $\mathcal{G}_{02}$. (c) $\mathcal{G}_{03}$ and (d) $\mathcal{G}_{04}$.

4.1.2. Using the geometric constructive approach of the vertex space (GCAV)

Since in this case we are dealing with a three-dimensional space, a cross-sectional plane should be considered in order to reduce the problem to a two-dimensional one. From a geometric inspection, it follows that a cross-sectional plane with $\mathbf{e}_3=\mathbf{e}_1\times\mathbf{e}_2$ as normal, called $\mathcal{X}$, results in a homogeneous section for the vertex space and leads to conventional geometric objects such as circles and lines. This helps to reduce the complexity of the computation and, to be precise, leads to an algorithm which consists in finding the intersections of some known geometric objects such as intersections of circles and lines. In the fixed frame, the vertex space, $\mathbf{w}_i$, can be formulated mathematically as follows:

$$\mathbf{w}_i=\mathbf{r}_i-\mathbf{Q}\mathbf{s}_i'. \tag{25}$$

The particular cross section $\mathcal{X}$ defined above, implies that the above expression should be multiplied by $\mathbf{Q}_\theta^{-1}$:

$$\mathbf{w}_i'=\mathbf{Q}_\theta^{-1}\mathbf{w}_i=\mathbf{Q}_\theta^{-1}\mathbf{r}_i-\mathbf{Q}_\phi\mathbf{s}_i', \tag{26}$$

where

$$\mathbf{Q}_\theta=\begin{bmatrix}\cos\theta & 0 & \sin\theta\\ 0 & 1 & 0\\ -\sin\theta & 0 & \cos\theta\end{bmatrix},\quad \mathbf{Q}_\phi=\begin{bmatrix}1 & 0 & 0\\ 0 & \cos\phi & -\sin\phi\\ 0 & \sin\phi & \cos\phi\end{bmatrix}. \tag{27}$$

In the above, one should be aware that $\mathbf{Q}=\mathbf{Q}_\theta\mathbf{Q}_\phi$ which is coming from the rotation sequence order as explained for Eq. (1). Each limb is constituted of two moving links and their corresponding motions are shown, respectively, in Figs. 8 and 9. From Fig. 8 it follows that

$$(z''-w_{iz}'')^2+(x''-w_{ix}'')^2=l_{1i}^2, \tag{28}$$

where $\mathbf{w}_i''=[w_{ix}'',w_{iy}'',w_{iz}'']^T$. It should be noted that components in the coordinate frame attached to the cross-sectional plane $\mathcal{X}$ with principal axes along $\mathbf{e}_1$ and $\mathbf{e}_2$ are distinguished by the "″" superscript. The cross section is followed along the x''-axis. The intervals of the vertex space are as follows:

$$\mathcal{B}_{1i}^V=\begin{cases}{}^{\mathrm{i}}\mathcal{X}_{\min}: w_{ix}''-l_{1i}\le x''\le w_{ix}''+l_{1i}: {}^{\mathrm{i}}\mathcal{X}_{\max},\\ {}^{\mathrm{i}}\mathcal{Y}_{\min}: w_{iy}''-l_{2i}-\dfrac{\Delta\rho_i}{2}\le y''\le w_{iy}''+l_{2i}+\dfrac{\Delta\rho_i}{2}: {}^{\mathrm{i}}\mathcal{Y}_{\max},\\ {}^{\mathrm{i}}\mathcal{Z}_{\min}: w_{iz}''-l_{1i}\le z''\le w_{iz}''+l_{1i}: {}^{\mathrm{i}}\mathcal{Z}_{\max}.\end{cases} \tag{29}$$

Note that $\mathcal{B}_{1i}^V$ in Eq. (29) can be regarded as a box in which the vertex space of limb i with structure $\Gamma=1$ is contained. The intersections of these boxes could be of great interest for the workspace determination using a node search method or interval analysis [24,31], where they have the potential to which will decrease the computational complexity.

Thus, for a given $x''=x_H''$, two solutions are in hand for z'', called z_{Hj}'', $j=\{1,2\}$, which are the z'' coordinates of the two sets of circles in Fig. 9. The equation representing the four circles in Fig. 9 can be expressed as follows:

$${}^1\mathcal{C}_i:(z''-z_{Hj}'')^2+\left(y''-w_{iy}''\pm\frac{\Delta\rho_i}{2}\right)^2=l_{2i}^2,\quad j=1,2. \tag{30}$$

Referring to Fig. 9, the expression of the four lines, called $\mathcal{L}_i$, tangent to the above circles having zero slopes is

$${}^1\mathcal{L}_i: z_{Hj}''\pm l_{2i}. \tag{31}$$

As it can be deduced from Fig. 9, the problem of obtaining the vertex space for $\Gamma=1$ is made equivalent to finding the intersections of the four circles connected by four lines, respectively, Eqs. (30) and (31), for a given cross-sectional plane $\mathcal{X}$, with respect to the interval given in Eqs. (29) and, finally, identifying which intersection is constituting the boundary of the vertex space. To do so, we resort to the algorithm presented in [35] for obtaining the constant-orientation workspace of general 6-DOF parallel mechanisms.

Thus the last step consists in obtaining all the circular arcs and lines defined by the intersection points found above and ordering these points. This should be accompanied by a checking procedure to identify the arcs and lines that constitute the boundary of the workspace. To do so, for a given curve, belonging to a given arc or line, a point lying on the curve is chosen, preferably not one of the end points. Then, using the IKP, it is verified whether this point has *boundary condition*, meaning that a little variation on this point leads to violating either the constraint inequalities of the IKP or the strokes of the prismatic actuator.

In summary, the following steps should be taken to determine the GCAV:

1. Formulating the vertex space, Eq. (25).
2. Applying the cross-sectional plane $\mathcal{X}$ to the vertex space, Eq. (26).
3. Obtaining the interval for which the cross-sectional plane $\mathcal{X}$ should be repeated, Eqs. (29).
4. Identifying circles, ${}^1\mathcal{C}_i$ and lines, ${}^1\mathcal{L}_i$, which are obtained by applying the cross-sectional plane $\mathcal{X}$ to the vertex space, Eqs. (30) and (31).
5. Finding all the intersection points among ${}^1\mathcal{C}_i$ and ${}^1\mathcal{L}_i$.
6. Identifying all the arcs and lines from the intersection points obtained above.
7. Considering an arbitrary point, called A_p, preferably the mid-point, for each arc and line obtained above.
8. Verifying whether A_p has *boundary condition* which, based on Eqs. (10)–(13), can be classified as follows:
   - $K_{1i}=0$;
   - $K_{2i}=0$ and $K_{3i}<0$;
   - $K_{3i}=0$ and $K_{2i}<0$;
   - $K_{2i}=0$ and $K_{3i}=0$;
   - $K_s=0$;

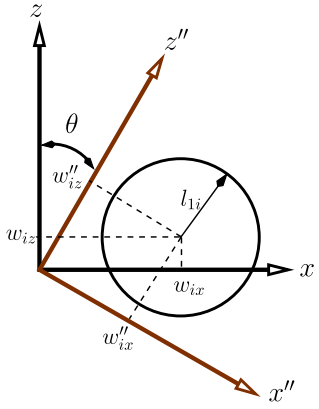

Fig. 8. Boundary generated by the first moving link for $\Gamma=1$.

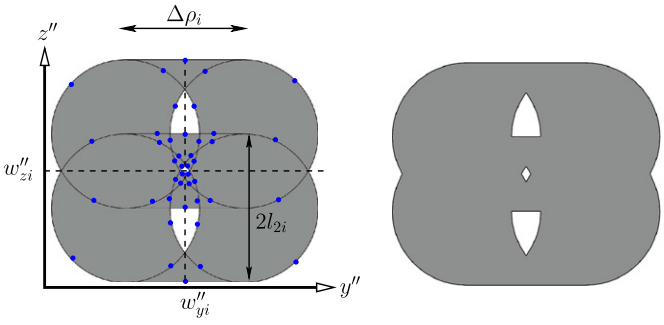

Fig. 9. Boundary generated by the second moving link for $\Gamma=1$ due to the motion generated by the first moving link.

- $K_{2i}=0$ and $K_{3i}>0$ but $K_s<0$ for the two solutions obtained from $K_{3i}>0$;
- $K_{3i}=0$ and $K_{2i}>0$ but $K_s<0$ for the two solutions obtained from $K_{2i}>0$.

Since a CAD model is presented for the vertex space of $\Gamma=1$ thus the vertex space obtained by using the above procedure is omitted. However, the above formulation given for GCAV will be used for obtaining the geometric constructive approach for the constant-orientation workspace, the so-called GCACOW. It should be noted that the GCAV introduced here can be regarded as a general approach for obtaining the vertex space of other parallel mechanisms whose vertex space is difficult to assess geometrically.

4.2. Topology of the vertex space for $\Gamma=0$

4.2.1. CAD-based modelling approach

The vertex space generated by a PRUR limb having a prismatic actuator along x-axis is equivalent to the vertex space generated by the same leg having the prismatic actuators along z-axis but rotated by $\pi/2$ around the axis of the prismatic actuator. Thus, only the vertex space for the limb with prismatic actuator in the direction of z-axis is elaborated.

Since in this case extruding a Bohemian dome in a CAD software is nearly impossible and the angle θ changes the topology of the vertex space, thus the CAD model of the vertex space of $\Gamma=0$ cannot be obtained directly and it is much more complicated than the $\Gamma=1$ one. Fig. 10 represents the CAD model of the vertex space for a limb with $l_{1i}=100$, $l_{2i}=160$ and $\Delta\rho_i=140$ for $\theta=\pi/6$. Therefore, a step-by-step procedure should be applied in order to construct different parts of the vertex space and finally assemble them to obtain the CAD model. These steps are presented in Appendix A to have an insight into the complexity of the CAD model of the vertex space of $\Gamma=0$. The complexity of modelling the vertex space of $\Gamma=0$ encourages us to use the so-called GCAV. Here, it can be concluded that the analysis of the workspace of a 5-DOF parallel mechanism for which at least one limb belongs to $\Gamma=0$ would be more constructive to be carried out using the GCAV, for the vertex space, and subsequently the GCACOW for the constant-orientation of the mechanism as a whole.

4.2.2. Using the geometric constructive approach of the vertex space (GCAV)

In the case of $\Gamma=0$, the topology of the vertex space is highly related to θ in such a way that the vertex space for $\theta=0$ could not be extended to other θ by a simple rotation. Moreover, for different θ the shape and characteristic of the holes vary. In contrast of $\Gamma=1$, in the case with $\Gamma=0$, as depicted in Fig. 10, there are three types of holes:

1. $\mathcal{H}_1^0$: Always exists, except for $\theta=\{0,\pi\}$. This hole is overall with respect to the following conditions:
   - if $(l_{1i}\cos\theta-\Delta\rho_i\sin\theta)>0$ the condition becomes: $l_{2i}>\sqrt{l_{1i}^2-(\Delta\rho_i/2)^2}-(\Delta\rho_i/2)\cos\theta$;
   - otherwise, the condition is: $l_{2i}>l_{1i}/\sin\theta$.
2. $\mathcal{H}_2^0$ and $\mathcal{H}_3^0$ exist when $\Delta\rho_i<2l_{1i}$:
   - $\mathcal{H}_2^0$ is overall when: $l_{1i}\sin(\theta-\beta)/\sin\theta<l_{2i}$ where $\beta=\arcsin(\Delta\rho_i\sin\theta/2l_{1i})$;
   - $\mathcal{H}_3^0$ is not overall but it would be larger when $\Delta\rho_i$ decreases.

The GCACOW requires the GCAV, thus in what follows the vertex space for $\Gamma=0$ is obtained using the GCAV. As each limb is constituted of two moving links, thus their corresponding motions are shown, respectively, in Figs. 11 and 12. Skipping mathematical details, the equations for the circles and lines in Fig. 11 are

$$\left(z''-w''_{iz}\pm\frac{\Delta\rho_i}{2}\sin\theta\right)^2+\left(x''-w''_{ix}\pm\frac{\Delta\rho_i}{2}\cos\theta\right)^2=l_{1i}^2, \tag{32}$$

$$z''\sin\theta+x''\cos\theta=w_{ix}\pm l_{1i}. \tag{33}$$

For a given $x''=x_H$, solving z'' from above, called z''_{Hj}, $j\geq 0$ provides the number of intersections which may vary for different $\mathcal{X}$, leading to the following circles and lines which are depicted in Fig. 12:

$${}^0\mathcal{C}_i:(z''-z''_{Hj})^2+(y''-w''_{iy})^2=l_{2i}^2, \tag{34}$$

$${}^0\mathcal{L}_i:y''=w'_{iy}\pm l_{2i}. \tag{35}$$

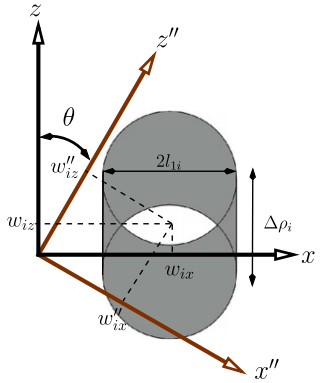

Fig. 11. Boundary generated by the first moving link for $\Gamma=0$.

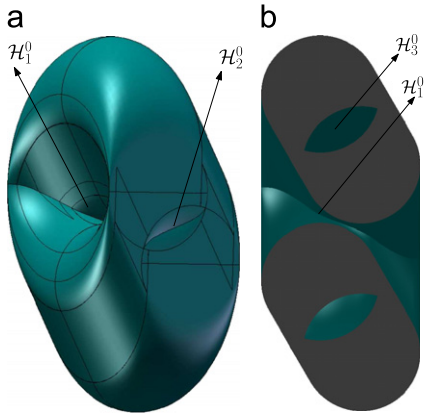

Fig. 10. CAD model of the vertex space of $\Gamma=0$ for $\theta=\pi/6$.

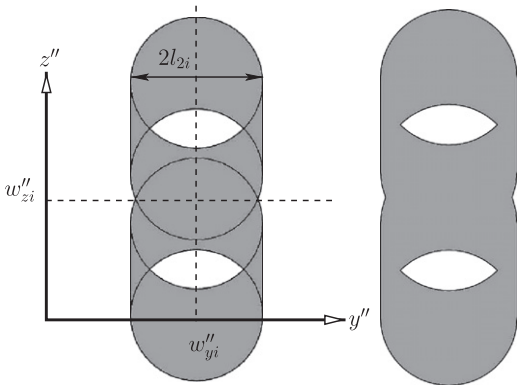

Fig. 12. Boundary generated by the second moving link for $\Gamma=0$ due to the first moving link.

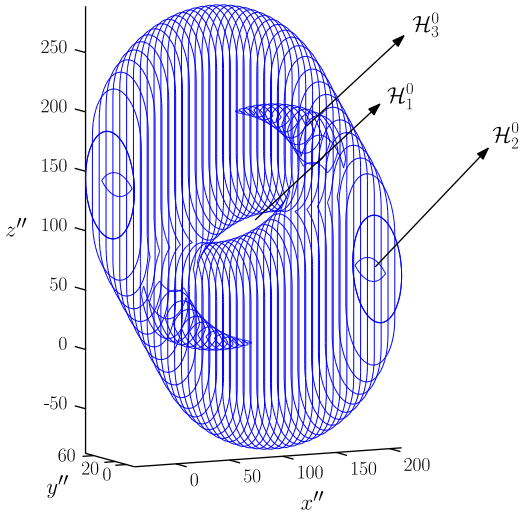

Fig. 13. Vertex space for $\Gamma=0$, prismatic actuator along z-axis and $\theta=\pi/6$, obtained by GCAV.

The intervals which include the vertex space are

$$\mathcal{B}_{0i}^{V}=\begin{cases} {}^{i}\mathcal{X}_{\min}: w''_{ix}-l_{1i}-\dfrac{\Delta\rho_i}{2}\,|\sin\theta| \le x'' \le w''_{ix}+l_{1i}+\dfrac{\Delta\rho_i}{2}|\sin\theta| : {}^{i}\mathcal{X}_{\max}, \\ {}^{i}\mathcal{Y}_{\min}: w''_{iy}-l_{2i} \le y'' \le w''_{iy}+l_{2i} : {}^{i}\mathcal{Y}_{\max}, \\ {}^{i}\mathcal{Z}_{\min}: w''_{iz}-l_{1i}-\dfrac{\Delta\rho_i}{2}\,|\cos\theta| \le z'' \le w''_{iz}+l_{1i}+\dfrac{\Delta\rho_i}{2}|\cos\theta| : {}^{i}\mathcal{Z}_{\max}. \end{cases} \tag{36}$$

Thus the problem of obtaining the vertex space for $\Gamma=0$ is made equivalent to finding the intersections of circles and lines, Eqs. (34) and (35), for a given cross-sectional plane $\mathcal{X}$ and identifying which arc or line is constituting the boundary of the vertex space. This can be done by resorting to the GCAV for $\Gamma=1$. Fig. 13 illustrates the vertex space for $\Gamma=0$ for a configuration for which $\theta=\pi/6$ and design parameters as $l_{1i}=100$, $l_{2i}=90$ and $\Delta\rho_i=140$.

4.3. Constant-orientation workspace

Reaching this step, having the topology of the vertex space and the GCAV, we pursue the study, respectively, on two fronts: CAD model and GCACOW.

4.3.1. CAD model of the constant-orientation workspace

Up to this point, the analysis of the vertex space in the preceding sections was arranged in such a way that allows to conduct the analysis of the constant-orientation workspace using both approaches mentioned above. Having in place the CAD model of the vertex space, the final step is to apply an offset vector to all the five vertex spaces which is in the direction opposite of the vector connecting the last joint of the limb to the mobile frame attached to the platform, $\mathbf{s}_i$. Finally, the workspace will be the intersection of the five offset vertex spaces. Fig. 15(a) shows the CAD model of the constant-orientation workspace of a parallel mechanism for which all the limbs belong to $\Gamma=1$, Fig. 14. Fig. B1(a) illustrates the CAD model of the constant-orientation workspace for the mechanism in Fig. 2 having some limbs which belong to $\Gamma=0$. As mentioned previously, the complexity of the CAD model of $\Gamma=0$ vertex space is the major deterrent to obtain easily the CAD model of the constant-orientation workspace of its corresponding parallel mechanism. However, since the CAD model of a mechanism having only $\Gamma=1$ is comparatively easier than the $\Gamma=0$, thus the CAD model of its corresponding parallel mechanism would be easier to obtain.

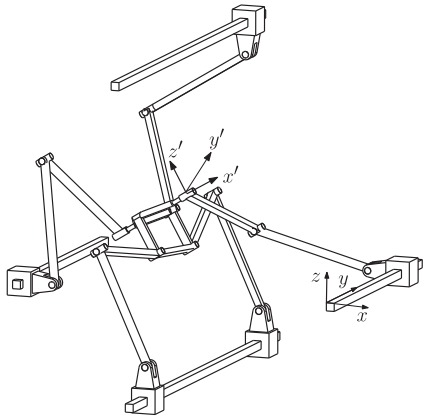

Fig. 14. Schematic representation of a 5-DOF (3T2R) parallel mechanism in which all limbs belong to $\Gamma=1$.

4.3.2. Geometrical constructive approach of the constant-orientation workspace (GCACOW)

Emphasis in this section is placed on GCACOW which can be regarded as the extension of GCAV for five limbs.

Based on the reasoning given for the GCAV, the following steps should be considered for the GCACOW:

1. Reduce the three-dimensional problem to a two-dimensional one by using the cross-sectional plane $\mathcal{X}$ defined in Eq. (26) for the five vertex spaces.
2. Consider a 5-PRUR comprising $n_g \le 5$ limbs having $\Gamma=0$ and $5-n_g$ limbs with $\Gamma=1$. The set of all the circles and lines segments obtained by applying the cross-sectional plane $\mathcal{X}$ for the five vertex spaces is defined, respectively, as $\mathcal{C}$ and $\mathcal{L}$:

$$\mathcal{C}=\{{}^{0}\mathcal{C}_1,\ldots,{}^{0}\mathcal{C}_{n_g},{}^{1}\mathcal{C}_1,\ldots,{}^{1}\mathcal{C}_{n_g-5}\}, \tag{37}$$

$$\mathcal{L}=\{{}^{0}\mathcal{L}_1,\ldots,{}^{0}\mathcal{L}_{n_g},{}^{1}\mathcal{L}_1,\ldots,{}^{1}\mathcal{L}_{n_g-5}\}. \tag{38}$$

3. The cross-sectional plane $\mathcal{X}$ is repeated along the x'' axis, x''_H, over the following interval:

$$\max\{{}^{i}\mathcal{X}_{\min}\} < x''_H < \min\{{}^{i}\mathcal{X}_{\max}\}, \quad i=1,\ldots,5. \tag{39}$$

   In the above, ${}^{i}\mathcal{X}_{\min}$ and ${}^{i}\mathcal{X}_{\max}$ were defined in Eqs. (29) and (36) for $\Gamma=1$ and $\Gamma=0$, respectively.
4. Having in place all the information concerning the circles (centre and radius) and lines (expression) from Eqs. (37) and (38), then upon considering the required interval for applying the cross-sectional plane $\mathcal{X}$, the following steps should be followed:
   (a) Finding the intersection points of all the circles in $\mathcal{C}$.
   (b) Finding the intersection points of circles, $\mathcal{C}$, with lines, $\mathcal{L}$.
   (c) Finding the intersection points between line segments, $\mathcal{L}$.
   (d) Ordering the intersection points found above. (Hint: The intersection points of circles are ordered using "atan2" function and intersection point of lines in ascending order);
5. Determining each arc or line constituting the boundary of the constant-orientation workspace by using the seven boundary conditions. To do so, the mid-point of the arc or line, is considered and substituted into the IKP of all the limbs. If the selected point satisfies the seven boundary conditions of its limb and IKP of other limbs, it will be a boundary of the workspace.

Fig. 15 represents the constant-orientation workspace for a given orientation of the platform of mechanism in Fig. 14 with geometric properties stated in Table 1. The constant-orientation workspace obtained by implementing the GCACOW, Fig. 15(b), is

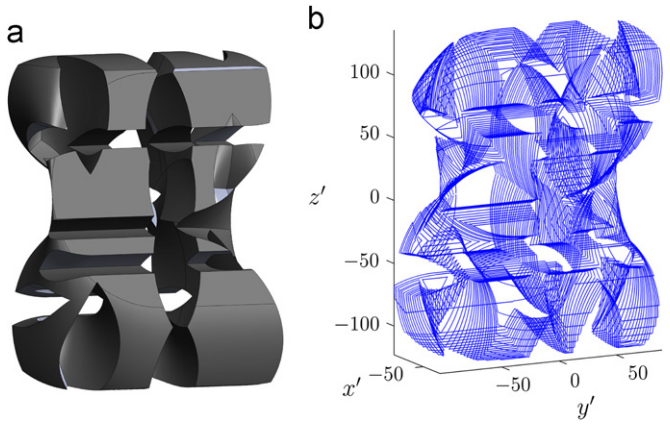

Fig. 15. Constant-orientation workspace for $\theta=\pi/3$ and $\phi=\pi/4$ for the design presented in Table B1. (a) CAD model. (b) GCACow.

Table 1
Geometric properties (in mm) assumed for the 5-PRUR parallel mechanism of Fig. 14.

i	$(\mathbf{r}_i)_x$	$(\mathbf{r}_i)_y$	$(\mathbf{r}_i)_z$	$(\mathbf{s}'_i)_x$	$(\mathbf{s}'_i)_y$	$(\mathbf{s}'_i)_z$
1	0	0	−70	0	0	0
2	0	0	70	0	40	0
3	−70	70	0	−20	20	20
4	70	70	0	20	20	20
5	0	140	70	0	40	20

compared with the one obtained by the CAD software, Fig. 15(a), as it can be observed that they are consistent. However, the consistency of the results is a must for the analysis but it is not the main concern of this paper. As pointed out previously, the main concern of this paper is to find a judicious synergy between the two approaches presented which can be summarized as follow. The CAD-based modelling approach is more suitable for the constant-orientation workspace analysis of the mechanisms with only $\Gamma=1$ since, in this case, the topology of the vertex space is invariant to the rotation of the mobile platform and only four possible cases are possible, Fig. 7. On the contrary, for the mechanisms with $\Gamma=0$ it turns out that the geometric constructive approach is more suitable, since the vertex space is not invariant to the rotation of the mobile frame and for each orientation set the vertex space should be regenerated in the CAD system which is a delicate task.

5. Volume of the constant-orientation workspace

As elaborated in [35], reaching this step the volume of the constant-orientation workspace can be obtained. The technique is based on the *Gauss divergence theorem* which can be applied to planar regions. As mentioned previously, the constant-orientation workspace for a given cross-section consists of the intersection of circles, resulting in some arcs, and lines. Thus, in order to compute the area, $A_{\mathcal{X}}$, for a given section obtained from the cross-sectional plane $\mathcal{X}$, the area generated by both arcs and lines should be considered, namely $A^a_{\mathcal{X}}$ and $A^l_{\mathcal{X}}$. Based on the results obtained in [35], apart from some minor modifications, the area created by an outer-arc – with centre as $[a^r_x,a^r_y]^T$, its radius r_a and the angle corresponding to the end points θ_1 and θ_2, (not to be confused with θ for DOF) – can be written as

$$A^a_{\mathcal{X}}=a^r_x r_a[\sin\theta_2-\sin\theta_1]+a^r_y r_a[\cos\theta_1-\cos\theta_2]+r^2_a[\theta_2-\theta_1]. \tag{40}$$

In what concerns the area created by the lines based on the formulation given in [35] for the *Gauss divergence theorem*, upon

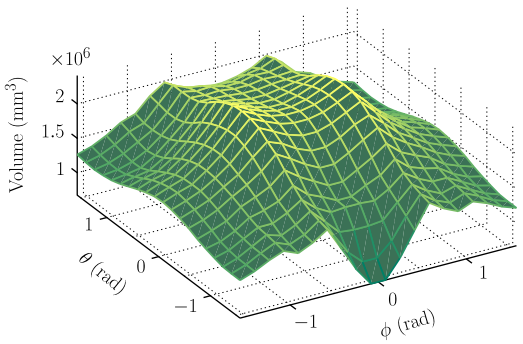

Fig. 16. Volume of the constant-orientation workspace with respect to (ϕ,θ) for the design presented in Table B1.

performing the integration, for the outer lines, it follows that

$$A^l_{\mathcal{X}}=\begin{cases}-y''_l(z''_u-z''_l) & \text{vertical line located in the left side of } w''_{iy},\\ y''_r(z''_u-z''_l) & \text{vertical line located in the right side of } w''_{iy},\\ -z''_l(y''_r-y''_l) & \text{horizontal line located in the lower side of } w''_{iz},\\ z''_u(y''_r-u''_l) & \text{horizontal line located in the upper side of } w''_{iy},\end{cases} \tag{41}$$

where (z''_l,z''_u) and (y''_r,y''_l) stand, respectively, for the z'' (lower and upper) and y'' (right and left) components of the line constituting the boundary of the constant-orientation workspace found by the GCACOW. For the inner arcs and lines the negative values of $A^a_{\mathcal{X}}$ and $A^l_{\mathcal{X}}$ should be, respectively, considered. Finally, the area of the cross section is

$$A_{\mathcal{X}}=\sum\left(\frac{A^a_{\mathcal{X}}+A^l_{\mathcal{X}}}{2}\right). \tag{42}$$

Finally, the volume of the workspace, V_w is obtained as follows:

$$V_w=\sum A_{\mathcal{X}}\Delta x, \tag{43}$$

where Δx is the distance between two successive cross-sections. The above formulation for computing the volume of the constant-orientation workspace is integrated inside the GCACOW. Fig. 16 represents the volume of the constant-orientation workspace with respect to two permitted orientations, (ϕ,θ), for the design presented in Table 1. Due to the symmetry of the proposed mechanism in Fig. 14 about the $\mathbf{e}_1$ axis, the corresponding surface for the volume of the workspace with respect to the two permitted angles, Fig. 16, is also symmetric with respect to the plane $\phi=0$ which is the angle of the rotation of the mobile platform around $\mathbf{e}_1$ axis.

6. Conclusion

This paper investigated the constant-orientation workspace of 5-DOF parallel mechanisms (3T2R) with a limb kinematic arrangement of type PRUR. From the results of the IKP, two types of 5-PRUR limbs were presented, $\Gamma=0$ and $\Gamma=1$, whose IKP and vertex spaces are different. Bohemian domes appeared in the geometrical interpretation of each limb and led to a CAD representation of the constant-orientation workspace. An algorithm, the so-called geometric constructive approach, was also proposed in order to find the boundary of the vertex space and the constant-orientation workspace which can be implemented in any computer algebra system. From the results obtained from both approaches, i.e., *CAD-based modelling* and *geometric constructive approach*, it can be deduced that there are host of advantageous to proceed geometrically the workspace analysis of such complex mechanisms. Moreover, both approaches used in this paper are complementary and, in general, there is no question of

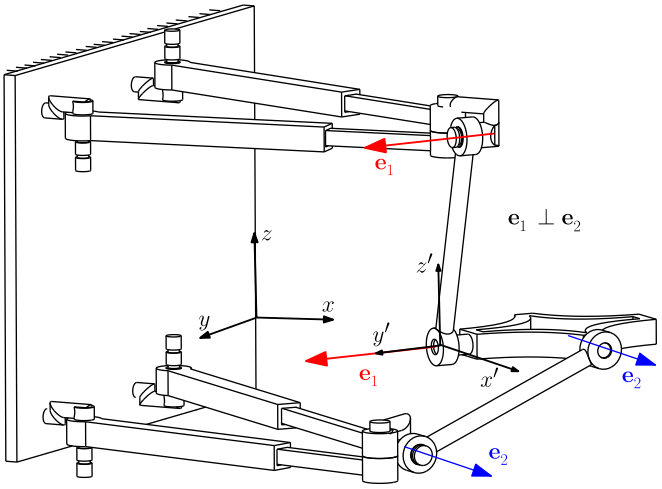

Fig. 17. CAD model of a 4-RPUR parallel mechanism for which the vertex of each limb is a Bohemian dome.

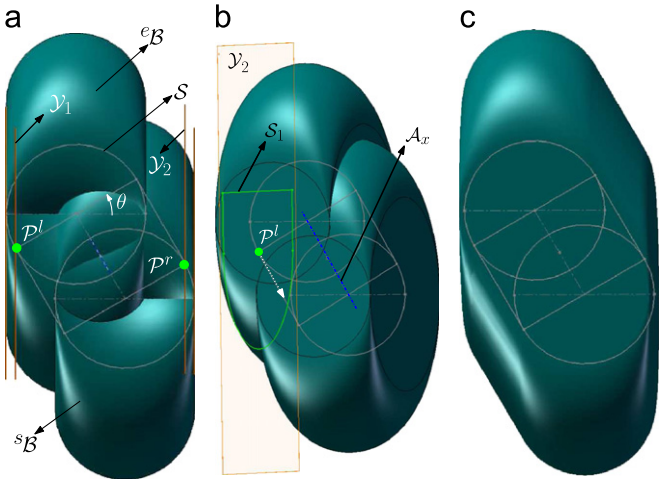

Fig. A1. The three steps for obtaining the main body of $\Gamma = 0$. (a) Step 1, (b) step 2 and (c) step 3. (For interpretation of the references to colour in this figure legend, the reader is referred to the web version of this article.)

superiority. However, in some particular designs, such as mechanisms with only $\Gamma = 1$, it is advantageous to obtain the constant-orientation workspace in a CAD system since the four possible vertex spaces are invariant to the rotational DOF of the platform and once obtained they can be readily applied for all orientation set of the platform. This is not the case for mechanism with $\Gamma = 0$ which makes the CAD approach more challenging. The geometric constructive approach made it possible to find the volume of the constant-orientation workspace by applying the *Gauss divergence theorem* and provided some insight into the optimum synthesis of 5-PRUR parallel mechanisms. The approach proposed in this paper can be regarded as an exhaustive guideline for the determination of the constant-orientation workspace of parallel mechanism whose the vertex space can be made equivalent to a Bohemian dome, such as the 4-RPUR parallel mechanism presented in Fig. 17. Ongoing works include the determination of the workspace upon considering the mechanical interferences and passive joint limits and the optimum design of such mechanisms.

Appendix A. Steps to obtain the CAD model of the vertex space for $\Gamma = 0$

Before entering into the details, we direct our attention to Fig. A1(a). As it is illustrated in the latter figure, the vertex space is limited by two Bohemian domes called ${}^{e}\mathcal{B}$ and ${}^{s}\mathcal{B}$ which are, respectively, the Bohemian domes generated by assuming the prismatic actuator positioned at $\rho_{\max i}$ and $\rho_{\min i}$. The procedure which should be followed in order to obtain the CAD model of the vertex space of $\Gamma = 0$ comprises three major steps:

1. *Obtaining the main body*: First, the sketch presented in Fig. A1(a), called $\mathcal{S}$, should be considered where the centre of the circles with radius as l_{1i} are the end and the start points of the prismatic actuator. In this step, we use this sketch in order to define two vertical planes, $\mathcal{Y}_1$ and $\mathcal{Y}_2$. These two planes pass through two points, namely, $\mathcal{P}^l$ and $\mathcal{P}^r$, as illustrated in Fig. A1(a).
   Having obtained $\mathcal{Y}_1$ and point $\mathcal{P}^l$ then the green sketch called $\mathcal{S}_1$, presented in Fig. A1(b), should be swept by $\Delta\rho_i$ along the axis called $\mathcal{A}_x$ which is the axis connecting the two circles of $\mathcal{S}$. It should be noted that the radius of the semi-circle in $\mathcal{S}_1$ is equal to l_{2i} and the rectangle should be as large as possible to cover the space between ${}^{s}\mathcal{B}$ and ${}^{e}\mathcal{B}$. The same reasoning should be applied for $\mathcal{Y}_3$ and point $\mathcal{P}^r$. Finally, the main body is the common intersection of the latter two objects with ${}^{s}\mathcal{B}$ and ${}^{e}\mathcal{B}$, as it is depicted in Fig. A1(c).
2. *Modelling the holes* $\mathcal{H}_1^0$, $\mathcal{H}_2^0$ *and* $\mathcal{H}_3^0$: Reaching this step, we need to divide the ${}^{e}\mathcal{B}$ and ${}^{s}\mathcal{B}$ into two parts. Each of the latter Bohemian domes, for instance ${}^{e}\mathcal{B}$, can be divided into two parts namely, the upper, ${}^{e}\mathcal{B}_u$, and the lower, ${}^{e}\mathcal{B}_l$, with respect to the symmetrical vertical plane. Similarly, the right and left

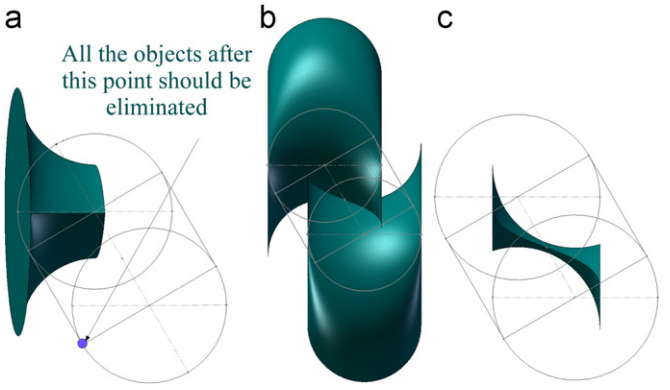

Fig. A2. First and second steps for obtaining $\mathcal{H}_1^0$: (a) ${}^{e}\mathcal{B}_{lu}^{r}$ (${}^{s}\mathcal{B}_{lu}^{r}$), (b) ${}^{e}\mathcal{B}^{u}$ and ${}^{s}\mathcal{B}^{l}$ together and (c) their intersection ${}^{es}\mathcal{B}^{lu}$.

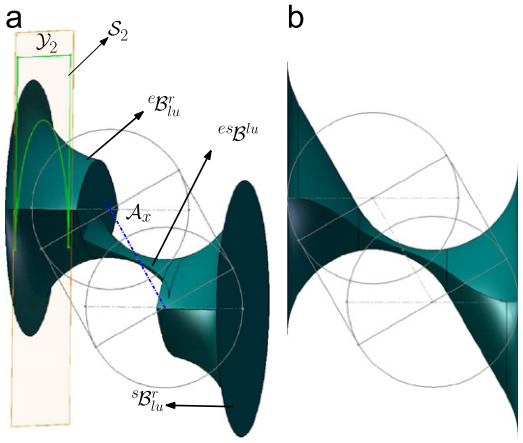

Fig. A3. Third step for $\mathcal{H}_1^0$: (a) assembling ${}^{e}\mathcal{B}_{lu}^{r}$, ${}^{s}\mathcal{B}_{lu}^{r}$ and ${}^{es}\mathcal{B}^{lu}$ and (b) the final result for $\mathcal{H}_1^0$.

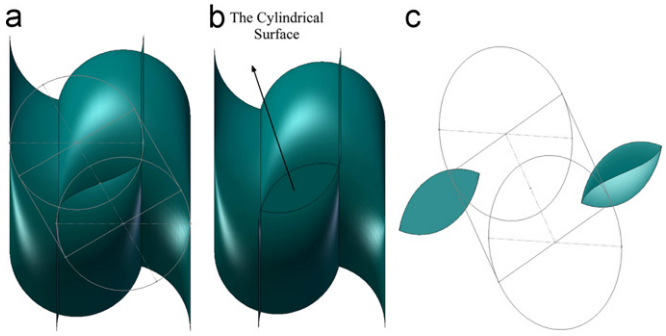

Fig. A4. Steps for obtaining $\mathcal{H}_2^0$: (a) intersection of ${}^{e}\mathcal{B}_l$ and ${}^{s}\mathcal{B}_u$, (b) adding the two cylindrical shape and (c) the final results for $\mathcal{H}_2^0$.

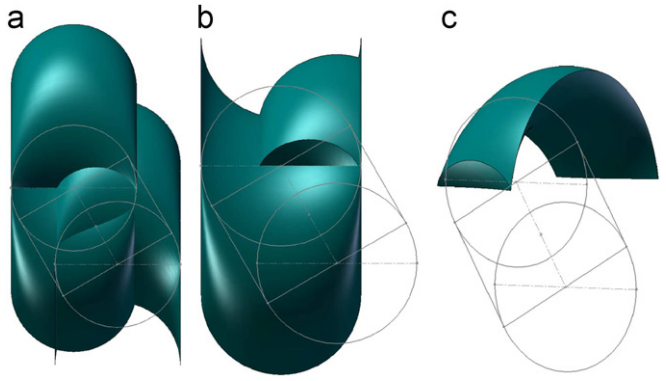

Fig. A5. Steps for obtaining $\mathcal{H}_3^0$: (a) putting together ${}^{s}\mathcal{B}_u$ and ${}^{e}\mathcal{B}_u$, (b) subtracting with ${}^{e}\mathcal{B}_l$ and (c) the final results for $\mathcal{H}_3^0$.

sides of ${}^{e}\mathcal{B}$ and ${}^{s}\mathcal{B}$ are, respectively, referred to as ${}^{e}\mathcal{B}^l$ and ${}^{e}\mathcal{B}^r$ with respect to the symmetrical horizontal plane. (The subscript u and l stand, respectively, for the upper and lower parts of a Bohemian dome and the superscript l and r represent, respectively, the left and right sides of a Bohemian dome.)

- Modelling $\mathcal{H}_1^0$: The procedure to find the $\mathcal{H}_1^0$ comprises three steps:
  First the hole appearing in the extreme sides of the vertex space should be obtained. To this end, we direct our attention to the one which is due to ${}^{e}\mathcal{B}$. To this end, the common intersection of ${}^{e}\mathcal{B}_l^r$ and ${}^{e}\mathcal{B}_u^r$ should be first considered, called ${}^{e}\mathcal{B}_{lu}^r$, Fig. A2(a). Similarly, one could find ${}^{s}\mathcal{B}_{lu}^r$. The second step consists in obtaining the common intersection of ${}^{e}\mathcal{B}^u$ and ${}^{s}\mathcal{B}^l$, called ${}^{es}\mathcal{B}^{lu}$, Fig. A2(c). In the case that the vertex space does not have an overall hole there will not be a common intersection for this step.
  The last step consists in assembling the objects found in the latter two steps and to apply nearly the same reasoning explained for the first step. As it can be seen from Fig. A3(a), a semi-circle with l_{2i} as radius tangent to the corresponding circular surface in $\mathcal{Y}_1$ accompanied with a large enough rectangular should be extruded along axis $\mathcal{A}_x$ by $\Delta\rho_i$ and should be removed from the objects obtained in the previous steps. The same reasoning should be repeated for $\mathcal{Y}_2$. The final results for the CAD model of $\mathcal{H}_1^0$ is presented in Fig. A3(b).
- Modelling $\mathcal{H}_2^0$: The second hole $\mathcal{H}_2^0$ is due to the space between ${}^{e}\mathcal{B}_l$ and ${}^{s}\mathcal{B}_u$. In order to obtain $\mathcal{H}_2^0$, one should first intersect two circles with radius l_{1i} where the centre is the start and the end points of the slider of the prismatic actuator. Then extruding by $2l_{2i}$, the common intersection surface of the latter two circles results in a volume which can be regarded as the intersection of two cylinders. Then by intersecting the latter shape with the lower part of ${}^{e}\mathcal{B}$, ${}^{e}\mathcal{B}_l$, and the upper part of ${}^{s}\mathcal{B}$, ${}^{s}\mathcal{B}_u$, leads to the $\mathcal{H}_2^0$ hole which is presented in Fig. A4(c).
- Modelling $\mathcal{H}_3^0$: The third hole, $\mathcal{H}_3^0$, can be obtained as follows: First, the intersection of ${}^{s}\mathcal{B}_u$, the upper part of ${}^{s}\mathcal{B}$, and the ${}^{e}\mathcal{B}_u$, the upper part of ${}^{e}\mathcal{B}$, should be found. The obtained objects should be subtracted from ${}^{e}\mathcal{B}_l$, the lower part of ${}^{e}\mathcal{B}$, which leads to $\mathcal{H}_3^0$, Fig. A5(c).

3. *Removing the above holes from the main body*: Finally, the vertex space can be obtained by removing the three holes obtained above from the main body. Fig. 10 represents the CAD model of the vertex space for a limb with $l_{1i}=100$, $l_{2i}=160$ and $\Delta\rho_i=140$ for $\theta=\pi/6$.

Appendix B. Constant-orientation workspace for the mechanism in Fig. 2 having some limbs that belong to $\Gamma=0$

Table B1 presents the geometric properties of the mechanism in Fig. 2. In this mechanism first, third and fifth limbs belong to $\Gamma=0$. Fig. B1(a) and (b) represents the constant-orientation workspace obtained by the CAD software and obtained by implementing the GCACOW, respectively. It can be observed that the constant-orientation workspace is highly irregular, and from Fig. B1 it can be inferred that *the constant-orientation workspace may have small isolated parts*.

Table B1
Geometric properties (in mm) assumed for the 5-PRUR parallel mechanism of Fig. 2.

i	$(\mathbf{r}_i)_x$	$(\mathbf{r}_i)_y$	$(\mathbf{r}_i)_z$	$(\mathbf{s}_i')_x$	$(\mathbf{s}_i')_y$	$(\mathbf{s}_i')_z$
1	140	0	70	0	−30	30
2	140	70	0	30	0	0
3	70	140	0	0	30	0
4	0	70	0	−30	0	0
5	0	140	70	0	30	30

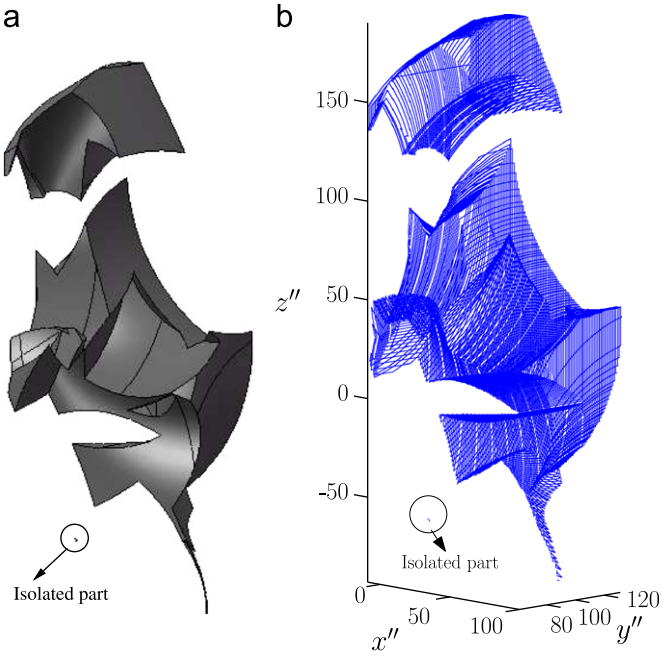

Fig. B1. Constant-orientation workspace for $\theta=\pi/6$ and $\phi=\pi/3$ for the design presented in Table 1. (a) CAD model. (b) GCACow.

References

[1] Kong X, Gosselin C. Type synthesis of parallel mechanisms, vol. 33. Heidelberg: Springer; 2007.

[2] Huang Z, Li QC. General methodology for type synthesis of symmetrical lower-mobility parallel manipulators and several novel manipulators. The International Journal of Robotics Research 2002;21(2):131–45.

[3] Fang Y, Tsai LW. Structure synthesis of a class of 4-DoF and 5-DoF parallel manipulators with identical limb structures. The International Journal of Robotics Research 2002;21(9):799–810.

[4] Huang Z, Li QC. Type synthesis of symmetrical lower-mobility parallel mechanisms using the constraint-synthesis method. The International Journal of Robotics Research 2003;22(1):59–79.

[5] Kong X, Gosselin C. Type synthesis of 5-DoF parallel manipulators based on screw theory. Journal of Robotic Systems 2005;22(10):535–47.

[6] Zhu SJ, Huang Z. Eighteen fully symmetrical 5-DoF 3R2T parallel manipulators with better actuating modes. The International Journal of Advanced Manufacturing Technology 2007;34(3):406–12.

[7] Bruzzone LE, Molfino RM. Special-purpose parallel robot for active suspension of ambulance stretchers. International Journal of Robotics and Automation 2003;18(3):121–30.

[8] Wang J, Gosselin C. Kinematic analysis and singularity representation of spatial five-degree-of-freedom parallel mechanisms. Journal of Robotic Systems 1997;14(12):851–69.

[9] Mbarek T, Barmann I, Corves B. Fully parallel structures with five degree of freedom: systematic classification and determination of workspace. In: Proceedings of mechatronics & robotics. Aachen; 2004. p. 990–6.

[10] Borras J, Thomas F, Torras C. A family of quadratically-solvable 5-SPU parallel robots. In: IEEE International Conference on Robotics and Automation. IEEE; 2010. p. 4703–8.

[11] Huang Z, Li QC. A decoupled 5-DoF symmetrical parallel mechanism. Patent pending, China, No. 01122274.3.

[12] Jin Q, Yang TL, Liu AX, Shen HP, Yao FH. Structure synthesis of a class of 5-DOF parallel robot mechanisms based on single opened-chain units. In: Proceedings of the 2001 ASME conferences, DETC2001/DAC21153, Pittsburgh, PA, 2001.

[13] Gao F, Peng B, Zhao H, Li W. A novel 5-DOF fully parallel kinematic machine tool. The International Journal of Advanced Manufacturing Technology 2006;31(1):201–7.

[14] Parallelmic 〈http://www.parallemic.org/〉.

[15] Piccin O, Bayle B, Maurin B, de Mathelin M. Kinematic modeling of a 5-DOF parallel mechanism for semi-spherical workspace. Mechanism and Machine Theory 2009;44(8):1485–96.

[16] Tale Masouleh M, Walter DR, Husty M, Gosselin C. Forward kinematics of the 5-DOF parallel mechanisms (3R2T) with identical limb structures using the linear implicitization algorithm. In: Proceeding of the 13th IFToMM world congress. Guanajuato, México; 2011.

[17] Tale Masouleh M, Husty M, Gosselin C. Forward kinematic problem of 5-PRUR parallel mechanisms using study parameters. In: Advances in robot kinematics: motion in man and machine. Springer; 2010. p. 211–21.

[18] Tale Masouleh M, Gosselin C, Husty M, Walter D. Forward kinematic problem of 5-RPUR parallel mechanisms (3T2R). Mechanism and Machine Theory 2011;46(7):945–59.

[19] Tale Masouleh M, Husty M, Gosselin C. A general methodology for the forward kinematic problem of symmetrical parallel mechanisms and application to 5-PRUR parallel mechanisms (3T2R). In: Proceedings of the 2010 ASME design engineering technical conferences, DETC2010-28222. Montreal, Canada: ASME; 2010.

[20] Tale Masouleh M, Gosselin C. Kinematic analysis and singularity representation of 5-RPRRR parallel mechanisms. In: Fundamental issues and future research directions for parallel mechanisms and manipulators, Montpellier, France; 2008. p. 79–90.

[21] Motevalli B, Zohoor H, Sohrabpour S. Structural synthesis of 5 DOFS 3T2R parallel manipulators with prismatic actuators on the base. Robotics and Autonomous Systems 2010;58(3):307–21.

[22] Krut S. Contribution à l'Études des Robot Parallèles Lègers, 3T-1R et 3T-2R, à Forts Débattement Angulaires. PhD thesis, Université Montpellier II, Montepllier; November 2002.

[23] Amine S, Tale Masouleh M, Caro S, Wenger P, Gosselin C. Singularity analysis of 5-DOF parallel mechanisms 3T2R using Grassmann–Cayley algebra. In: Proceedings of the 13th IFToMM world congress. Guanajuato, México; 2011.

[24] Merlet JP. Parallel robots. Springer; 2006.

[25] Gherman B, Vaida C, Pisla D, Plitea N, Gyurka B, Lese D, et al. Singularities and workspace analysis for a parallel robot for minimally invasive surgery. In: IEEE international conference on automation quality and testing robotics (AQTR), vol. 1; 2010. p. 1–6.

[26] Jin Y, Chen I-M, Yang G. Workspace evaluation of manipulators through finite-partition of SE (3). Robotics and Computer-Integrated Manufacturing 2011;27(4):850–9.

[27] Wang Z, Ji S, Li Y, Wan Y. A unified algorithm to determine the reachable and dexterous workspace of parallel manipulators. Robotics and Computer-Integrated Manufacturing 2010;25(5):454–60.

[28] Bi ZM, Lang SYT. Joint workspace of parallel kinematic machines. Robotics and Computer-Integrated Manufacturing 2009;25(1):57–63.

[29] Bohigas O, Ros L, Manubens M. A complete method for workspace boundary determination. In: Advances in robot kinematics: motion in man and machine. Springer; 2010. p. 329–38.

[30] Snyman JA, Du Plessis L, Duffy J. An optimization approach to the determination of the boundaries of manipulator workspaces. Journal of Mechanical Design 2000;122:447.

[31] Chablat D, Wenger P, Merlet JP. Workspace analysis of the orthoglide using interval analysis. In: 8th international symposium on advances in robot kinematics. Kluwer Academic Publishers; 2002.

[32] Merlet JP. Determination of 6D workspaces of Gough-type parallel manipulator and comparison between different geometries. The International Journal of Robotics Research 1999;18(9):902.

[33] Bonev IA. Geometric analysis of parallel mechanisms. PhD thesis, Laval University, Quebec, QC, Canada; October 2002.

[34] Bonev IA, Ryu J. A geometrical method for computing the constant-orientation workspace of 6-PRRS parallel manipulators. Mechanism and Machine Theory 2001;36(1):1–13.

[35] Gosselin C. Determination of the workspace of 6-DOF parallel manipulators. ASME Journal of Mechanical Design 1990;112(3):331–6.

[36] Mayer St-Onge B, Gosselin CM. Logiciel d'Aide la conception de plates-formes de mouvement d'Architecture parallèle. In: CCToMM symposium on mechanisms, machines, and mechatronics (SM3), Saint-Hubert, QC, Canada; 2001.

[37] Gosselin C, Tale Masouleh M, Duchaine V, Richard PL, Foucault S, Kong X. Parallel mechanisms of the multipteron family: kinematic architectures and benchmarking. In: IEEE international conference on robotics and automation, Roma, Italy; 2007. p. 555–60.

[38] Bonev IA, Gosselin CM. Geometric algorithms for the computation of the constant-orientation workspace and singularity surface of a special 6-RUS parallel manipulator. In: Proceedings of the 2000 ASME design engineering technical conferences, DETC2002/MECH-34257, Montreal, QC, Canada; 2002.